THE JOURNAL OF BIOLOGICAL CHEMISTRY
Vol. 277, No. 38, Issue of September 20, pp. 35378–35385, 2002

Printed in U.S.A.

Identification of a Non-canonical Tyrosine-based Endocytic Motif in an Ionotropic Receptor*[S]

Received for publication, May 16, 2002
Published, JBC Papers in Press, July 8, 2002, DOI 10.1074/jbc.M204844200

Stephen J. Royle, Laura K. Bobanović, and Ruth D. Murrell-Lagnado‡

From the Department of Pharmacology, University of Cambridge, Tennis Court Road, Cambridge CB2 1PD, United Kingdom

Rapid modulation of the surface number of certain ionotropic receptors is achieved by altering the relative rates of insertion and internalization. These receptors are internalized by a clathrin-mediated pathway; however, a motif that is necessary for endocytosis of ionotropic receptors has not yet been identified. Here, we identified a motif that is required for constitutive and agonist-regulated internalization of the ionotropic $P2X_4$ receptor. Three amino acids in the C terminus of $P2X_4$ (Tyr^{378}, Gly^{381}, and Leu^{382}) compose a non-canonical tyrosine-based sorting signal of the form *YXX*GL. We found that $P2X_4$ protein was present in clathrin-coated vesicles isolated from rat brain and that a glutathione *S*-transferase fusion of the $P2X_4$ C terminus pulled down the adaptor protein-2 complex from brain extract. Mutation of either the tyrosine-binding pocket of the μ2 subunit of adaptor protein-2 or the *YXX*GL motif in the receptor C terminus caused a decrease in receptor internalization and a dramatic increase in the surface expression of $P2X_4$ receptors. The *YXX*GL motif represents a non-canonical tyrosine-based sorting signal that is necessary for efficient endocytosis of the $P2X_4$ receptor. Similar motifs are present in other receptors and may be important for the control of their functional expression.

A cell can sense extracellular stimuli by using receptors at the surface to transduce these messages into electrical or chemical signals. An emerging picture for ionotropic receptors is that rapid modulation of their surface number can control the response to a given stimulus. This is of considerable interest because, for ionotropic receptors in synaptic membranes, this may underlie the changes in synaptic strength observed during long-term potentiation and depression (1–3). Constitutive endocytosis and recycling of ionotropic receptors are likely to be essential for rapid modulation of surface receptor number because, by changing the relative rates of receptor internalization and insertion, the cell can alter the receptor density (4, 5). For ionotropic receptors, the constitutive internalization of AMPA,[1] $P2X_4$, and γ-aminobutyric acid type A receptors has been demonstrated (6–8).

The mechanism of internalization of transmembrane proteins by clathrin-mediated endocytosis is well established. Proteins destined for internalization are concentrated in clathrin-coated pits before being "pinched off" to form an endocytic vesicle (9). Most cargo proteins are recruited to coated pits via an interaction with their intracellular domains and adaptor protein-2 (AP-2). These interactions typically involve tyrosine-based sorting signals in the intracellular domain of the cargo protein and the medium (μ2) subunit of AP-2 (10). Generally, tyrosine-based signals are of the form NP*X*Y or Y*XX*Ø (where *X* is any amino acid and Ø is an amino acid with a bulky hydrophobic side chain) (11). Y*XX*Ø signals bind to μ2 in an extended conformation, with the Tyr and Ø residues fitting into two hydrophobic pockets in subdomain A of μ2 (12).

The mechanism of constitutive internalization of ionotropic receptors in neurons is thought to be similar to classical clathrin-mediated endocytosis in being dependent on both clathrin and dynamin (6, 13–15). Other molecular details of this process are less clear, however. For example, do recycling ionotropic receptors link to the endocytic pathway via canonical Y*XX*Ø motifs? Regions of the AMPA receptor protein that are important for endocytosis have been identified (14), and an interaction with AP-2 has been shown for both AMPA and γ-aminobutyric acid type A receptors (6, 8). However, endocytic motifs for these receptors have not yet been described (2). A canonical tyrosine-based sorting motif was identified for the *N*-methyl-D-aspartic acid receptor (16), but this receptor does not constitutively internalize in mature neurons (14, 17). The purpose of this study therefore was to analyze how a recycling ionotropic receptor links to the endocytic pathway.

P2X receptors are ionotropic receptors activated by extracellular ATP (18). Previously, we have shown that P2X receptor trafficking is subunit-specific (7). $P2X_4$ receptors are rapidly cycled between the plasma membrane and endosomal compartments. $P2X_2$ receptors are, by contrast, stably expressed at the surface. Herein, we describe the endocytic motif of the $P2X_4$ receptor. We found that it is a novel non-canonical tyrosine-based sorting signal. Mutation of the motif caused an inhibition of both constitutive and agonist-regulated endocytosis of the receptor, confirming a common mechanism for these pathways. Perturbation of $P2X_4$ receptor endocytosis resulted in a large increase in the pool of functional receptors at the cell surface. Similar motifs are found in other receptor proteins, suggesting that this motif may be important for the constitutive internalization and modulation of the surface number of other receptor and ion channel types.

EXPERIMENTAL PROCEDURES

DNA Constructs—The construction of enhanced green fluorescent protein (GFP)- and epitope-tagged $P2X_4$ and $P2X_2$ receptors has been

* This work was supported by the Biotechnology and Biological Sciences Research Council and The Wellcome Trust. The costs of publication of this article were defrayed in part by the payment of page charges. This article must therefore be hereby marked "*advertisement*" in accordance with 18 U.S.C. Section 1734 solely to indicate this fact.

[S] The on-line version of this article (available at *http://www.jbc.org*) contains Supplemental Fig. 1.

‡ To whom correspondence should be addressed. Tel.: 44-1223-334011; Fax: 44-1223-334040; E-mail: rdm1003@cam.ac.uk.

[1] The abbreviations used are: AMPA, α-amino-3-hydroxy-5-methylisoxazole 4-proprionate; AP-2, adaptor protein-2; GFP, green fluorescent protein; GST, glutathione *S*-transferase; HEK293, human embryonic kidney 293; PBS, phosphate-buffered saline; FITC, fluorescein isothiocyanate; CCV, clathrin-coated vesicle; MES, 4-morpholineethanesulfonic acid; GluR, glutamate receptor.

described previously (7). Chimeric receptors and point mutations in $P2X_4$ were made by two-step PCR using GFP-tagged receptors as a template. For expression of either wild-type or epitope-tagged P2X receptors, the coding sequences of $P2X_4$-GFP constructs were amplified to reintroduce the stop codon and an *Xba*I site. The subcloning of these fragments into wild-type or epitope-tagged $P2X_4$ constructs excised the coding sequence of GFP. The sites of crossover for $P2X_4$(2C) and $P2X_2$(4C) receptors were Leu^{358}–Thr^{354} and Leu^{353}–Tyr^{359}, respectively. Deletion constructs were made by PCR. The first residues following the starting methionine were Val^7 and Asp^{16} for NΔ5 and NΔ14, respectively. For CΔ28, CΔ14, and CΔ7, the final residues before the linker between the receptor and GFP were Cys^{360}, Tyr^{374}, and Gly^{381}, respectively. In the case of CΔ7, Leu^{382} was effectively replaced by proline in the linker region, and no significant change in trafficking was observed when compared with wild-type $P2X_4$-GFP.

Rat μ2 (AP50) cDNA in pGAD424, a kind gift of Dr. M. S. Robinson (Cambridge Institute of Medical Research, Cambridge, UK), was amplified and subcloned into pcDNA3.1 at *Hin*dIII and *Xba*I sites. The dominant-negative μ2 subunit was made by sequentially mutating D176A and W421A using two-step PCR (19). For expression of a fusion protein of glutathione *S*-transferase (GST) with the C terminus of $P2X_4$ (GST-4C), the C-terminal region of $P2X_4$ was amplified by PCR and subcloned into pGEX-2T at *Bam*HI and *Eco*RI sites. The sequences of all amplified regions were verified by automated DNA sequencing.[2]

Cell Culture and Transfection—Primary cultures of olfactory bulb neurons were prepared from 3–4-day-old Wistar rats using a modified method for culturing hippocampal neurons (7, 20). Human embryonic kidney 293 (HEK293) cells were maintained in Dulbecco's modified Eagle's medium/nutrient mixture F-12 containing 10% fetal bovine serum and 100 units/ml penicillin/streptomycin at 37 °C and 5% CO_2. HEK293 cells stably transfected with μ2 constructs were cultured in the same medium supplemented with 0.6 mg/ml Geneticin sulfate (G418).

Olfactory bulb neurons were transfected at 10–21 days *in vitro* using a modified calcium phosphate method (7). HEK293 cells were plated onto poly-D-lysine-treated coverslips and transiently transfected 12 h later using the same method with slight modifications. The amount of DNA used to form a precipitate was 3 μg (in 100 μl of $CaCl_2$/100 μl of 2× HEPES-buffered saline), and cells were kept with the precipitate for 6 h. For stable transfection, HEK293 cells were transfected using the calcium phosphate method. Culture medium containing G418 was added 24 h later, and stable cell lines contained a pool of resistant colonies.

Electrophysiological Recordings—Standard whole-cell recordings (21) were performed at room temperature using an Axopatch 200A amplifier (Axon Instruments, Inc.). Patch pipettes (3–8 megaohms) were pulled from thick-walled borosilicate glass (GC150F-10, Harvard Apparatus, Inc.) and filled with solution containing 125 mM potassium gluconate, 1 mM $MgCl_2$, and 10 mM HEPES (pH 7.3). The extracellular solution was composed of 140 mM NaCl, 5 mM KCl, 2 mM $CaCl_2$, 1 mM $MgCl_2$, 10 mM D-glucose, and 10 mM HEPES (pH 7.3). ATP-induced responses were measured at −30 mV.

Whole-cell currents were low pass-filtered at 2 kHz and digitized at 10 kHz. ATP was applied locally using a Picospritzer II (Parker Instrumentation). To ensure delivery of drug, 0.05% (w/v) fast green was used. (Local applications of 1% fast green induced no response.) To visualize cells expressing P2X receptors, cells were cotransfected with GFP (0.5 μg of pEGFP-N1 vector was included in the precipitate) and observed under a microscope with an epifluorescence attachment (Nikon Inc.). Untransfected cells and cells expressing GFP alone were found to have no inward current in response to application of ATP. Acquisition was performed using HEKA Pulse Version 8.30, and data were subsequently analyzed using IgorPRO Version 3.16. Statistical analyses were performed with Student's unpaired *t* test using InStat software (Version 2.01, GraphPAD Software).

Cell Biology and Live Labeling Immunofluorescence Protocols—All cells were used 48 h post-transfection. For analysis of the subcellular distribution of GFP-tagged receptors, cells were fixed in 3% paraformaldehyde and 4% sucrose in phosphate-buffered saline (PBS; 1.5 mM NaH_2PO_4, 8 mM Na_2HPO_4, and 145 mM NaCl (pH 7.3)) for 10 min at 4 °C. Coverslips were washed with PBS and mounted onto slides with Vectashield (Vector Laboratories, Inc.) as a mounting medium.

The basic protocol for live labeling of AU5-tagged receptors expressed in HEK293 cells or cultured neurons was as follows. Anti-AU5 antibody in serum- and supplement-free culture medium was applied for 30 min at 37 °C. Cells were then washed five times with PBS and fixed in paraformaldehyde. In all experiments, prior to application of antibodies, nonspecific sites were blocked using PBS containing 4% normal goat serum and 3% bovine serum albumin (blocking buffer). Antibodies were prepared at their final concentration in blocking buffer.

To detect surface and internalized receptors, AU5-labeled receptors at the surface of fixed non-permeabilized cells were stained with a Cy3 (indocarbocyanine)-conjugated anti-mouse secondary antibody for 2 h at room temperature. Cells were then washed five times with PBS, permeabilized with 0.1% Triton X-100 in PBS, and stained with a fluorescein isothiocyanate (FITC)-conjugated anti-mouse secondary antibody for 2 h at room temperature to visualize prelabeled internalized receptors.

To determine the ratio between surface receptors and the total receptor population, non-permeabilized cells were stained with a Cy3-conjugated anti-mouse secondary antibody. After permeabilization, cells were stained for total $P2X_4$ population using anti-$P2X_4$ antibody for 2 h at room temperature and then a FITC-conjugated anti-rabbit secondary antibody for 2 h at room temperature.

To examine the effects of ATP on receptor internalization, neurons were labeled as described above, washed five times with buffer, and subsequently incubated for 15 min at 37 °C with or without ATP (100 μM) in extracellular solution (see "Electrophysiological Recordings"). Prelabeled receptors at the surface and internalized receptors were detected as described above.

To measure transferrin uptake, HEK293 cells were incubated in serum-free culture medium for 30 min at 37 °C. Following three washes, coverslips were incubated for 15 min at 37 °C in serum-free medium containing transferrin/Alexa 546 (100 μg/ml; Molecular Probes, Inc.). Cells were then washed, fixed, and mounted.

Image Collection and Analysis—Fluorescence was visualized using a Zeiss Axiovert LSM510 confocal microscope with a ×63 oil immersion objective. For FITC/Cy3 double labeling, FITC and Cy3 were excited at 2 and 20% of 488 and 543 nm laser power, respectively. Images where the confocal plane was focused on the middle of the cell (0.7-μm thickness) were taken at 0.14 μm/pixel. For transferrin uptake, Alexa 546 was excited at 60% of 543 nm laser power, and 1-μm-thick images were taken at 0.07 μm/pixel. Identical acquisition parameters were used for image capture of individual experiments.

Tagged image file format images were imported into NIH Image Version 1.62. Cells were outlined, and mean pixel values for each channel were obtained for a region over the cell soma. Pixel values were on an 8-bit scale (2^8 = 256, 0–255).

For internalization experiments, green (FITC) fluorescence intensity indicative of internalized receptors was divided by AU5-labeled (red + green) fluorescence intensities. Similarly for surface expression experiments, red (Cy3) fluorescence intensity indicative of surface receptors was divided by total $P2X_4$ (green) fluorescence intensity. For both types of experiments, measurements were normalized to control values.

For analysis of puncta frequency, single confocal images (2-μm thickness) were taken of the processes of transfected neurons (≥10 μm from the cell soma). For counts of puncta frequency, a 1-pixel-thick line was drawn along neuronal processes and measured. Puncta of GFP-tagged receptors or of internalized AU5-labeled receptors were defined by being discrete areas of fluorescence with an intensity that was greater than twice that of the background. Data are presented as puncta/10 μm of neurite.

Experiments were repeated at least three times; and each time, data were analyzed for cells from two separate coverslips. In each experiment, the data were normalized to control cells. The *n* value given refers to the number of cells analyzed. All data are presented as the means ± S.E. Histograms and plots were done using IgorPRO Version 3.16 software. Statistical analyses were performed by Student's unpaired *t* test or analysis of variance with Bonferroni's or Student-Newman-Keul's post hoc comparison using InStat software (Version 2.01). Levels of statistical significance are indicated in the figure legends.

Western Blotting and Protein-Protein Interaction Assays—Clathrin-coated vesicles (CCVs) were prepared as described previously (22). Briefly, whole brains from adult Wistar rats were homogenized in an equal volume of buffer containing 0.1 mM MES, 1 mM EGTA, 0.5 mM $MgCl_2$, 0.02% sodium azide (pH 6.5), and 0.5 mM phenylmethylsulfonyl fluoride. Debris and nuclei were removed by centrifugation at 5400 × *g* for 40 min. Coated vesicles were recovered from the supernatant by ultracentrifugation at 125,000 × *g* for 1 h. The pellet was resuspended in 4 volumes and then mixed with an equal volume of sucrose/Ficoll solution. Centrifugation at 28,000 × *g* for 40 min pelleted membranes and cytoskeletal elements (P3). The supernatant was diluted with 3

[2] The sequences of all oligonucleotide primers used are available upon request.

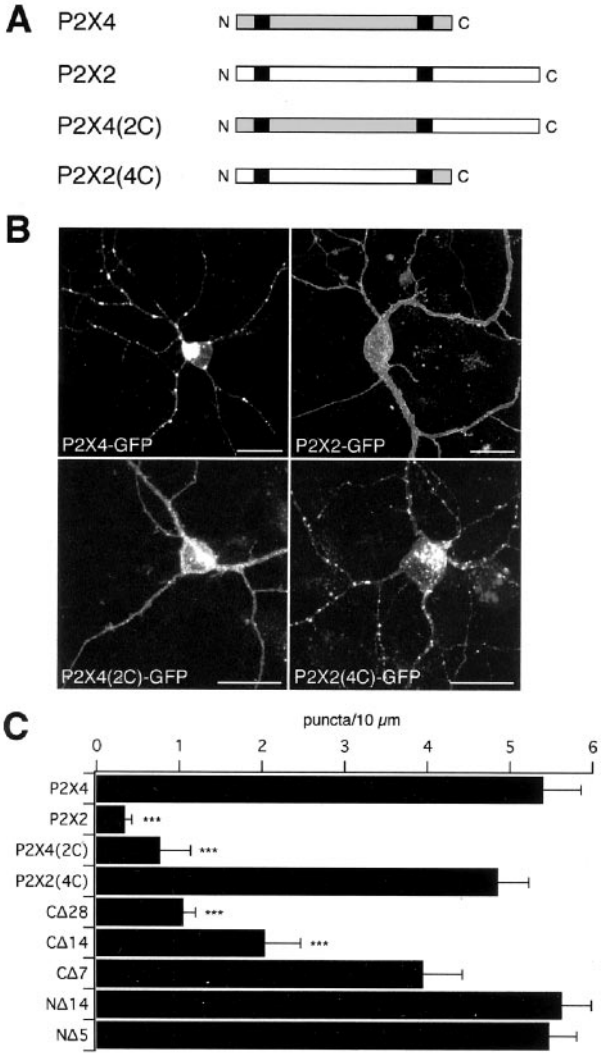

FIG. 1. **The C terminus of P2X$_4$ is necessary for receptor trafficking.** *A*, schematic representation of P2X receptor constructs. The P2X$_4$ and P2X$_2$ sequences are shown as *gray* and *white boxes*, respectively. *Black boxes* represent transmembrane domains. *B*, subcellular distribution of GFP-tagged wild-type and chimeric receptors in neurons. *Scale bars* = 20 μm. *C*, histogram showing the mean frequency of receptor-positive puncta in the neurites of transfected neurons. Puncta frequency for wild-type P2X$_4$ and P2X$_2$ receptors is shown compared with that for chimeric receptors and for P2X$_4$ receptors with deletions at the C and N termini (n = 3–10). All constructs were GFP-tagged at the C terminus. ***, $p < 0.001$.

volumes of buffer and sedimented by ultracentrifugation at 125,000 × *g* for 1 h. Smooth vesicles were largely in the supernatant, whereas CCVs were recovered from the pellet. Fractions were separated by 10% SDS-PAGE (23), transferred to nitrocellulose membranes, and probed with various primary antibodies and appropriate horseradish peroxidase-conjugated secondary antibodies, followed by detection with ECL (Amersham Biosciences, Buckinghamshire, UK). Membranes were stained with Ponceau S to check equivalent loading of samples.

GST or GST-4C was expressed in *Escherichia coli* strain BL21 and purified according to standard procedures. Pull-down assays were performed using rat brain extract as described previously (8). Precipitated material was eluted with Laemmli buffer, separated by SDS-PAGE, and analyzed by Western blotting.

Antibodies and Reagents—The following primary antibodies were used: affinity-purified mouse monoclonal anti-AU5 (5 μg/ml; BAbCO) and anti-α-adaptin (clone 100/2; 1:200) and rabbit polyclonal anti-P2X$_4$ (6 or 1.2 μg/ml for immunoblotting; Alomone), anti-P2X$_2$ (1.5 μg/ml; Alomone), anti-P2X$_7$ (1.5 μg/ml; Alomone), and anti-GluR1 (0.1 μg/ml; Chemicon International, Inc.). FITC- or Cy3-conjugated goat anti-mouse or anti-rabbit IgG secondary antibodies (1:250; Jackson ImmunoResearch Laboratories, Inc.) were used for immunocytochemistry.

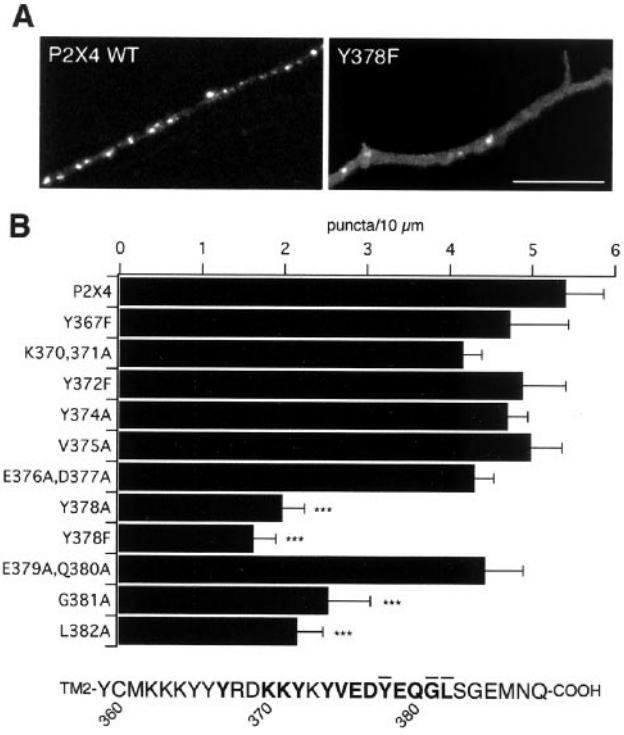

FIG. 2. **Identification of residues involved in P2X$_4$ receptor trafficking.** *A*, representative confocal images used for analysis of puncta frequency. *Scale bar* = 10 μm. *B*, histogram showing the mean frequency of receptor-positive puncta in neurites of transfected neurons. Puncta frequency for the GFP-tagged wild-type (*WT*) P2X$_4$ receptor is shown compared with that for GFP-tagged mutant receptors (n = 4–13). The sequence of the intracellular C terminus of P2X$_4$ is shown below. Residues that were mutated are shown in *boldface*, and those that produced a significant decrease in puncta frequency are *overlined*. *TM2*, transmembrane domain 2. ***, $p < 0.001$.

Horseradish peroxidase-conjugated anti-mouse or anti-rabbit secondary antibodies (1:10000; Amersham Biosciences) were used for Western blotting. Unless otherwise stated, all reagents were obtained from Sigma or Invitrogen.

RESULTS

Identification of a Region Required for Internalization of P2X$_4$ Receptors—P2X$_4$ receptors undergo constitutive and regulated endocytosis, whereas P2X$_2$ receptors do not (7). When heterologously expressed in neurons, P2X$_4$ receptors are distributed in discrete intracellular puncta throughout neurites, whereas P2X$_2$ receptors are more uniformly distributed at the plasma membrane. Many of the puncta of P2X$_4$ receptors colocalize with a marker for early endosomes.

To identify the molecular determinants of trafficking, we took advantage of this difference between the two receptor subtypes and generated chimeras between P2X$_2$ and P2X$_4$ in which the C termini were switched (Fig. 1*A*). GFP-tagged receptors were expressed in cultured neurons, and their subcellular distributions were visualized by confocal microscopy. Tagging the wild-type receptors with GFP at their C termini does not substantially alter their subcellular distribution or functional expression (7). The trafficking of the chimeras was largely determined by their C-terminal region, with the distribution of the P2X$_2$(4C) chimera resembling that of P2X$_4$ receptors and, conversely, that of the P2X$_4$(2C) chimera resembling P2X$_2$ receptors (Fig. 1*B*). The frequency of fluorescent puncta along the processes provides a comparative measure of receptor internalization. P2X$_4$ had a frequency of 5.41 ± 0.46 puncta/10 μm (Fig. 1*C*), similar to that of the P2X$_2$(4C) chimeric receptor (4.86 ± 0.37 puncta/10 μm). In contrast, the frequency of puncta for P2X$_2$ and the P2X$_4$(2C) chimera was much lower

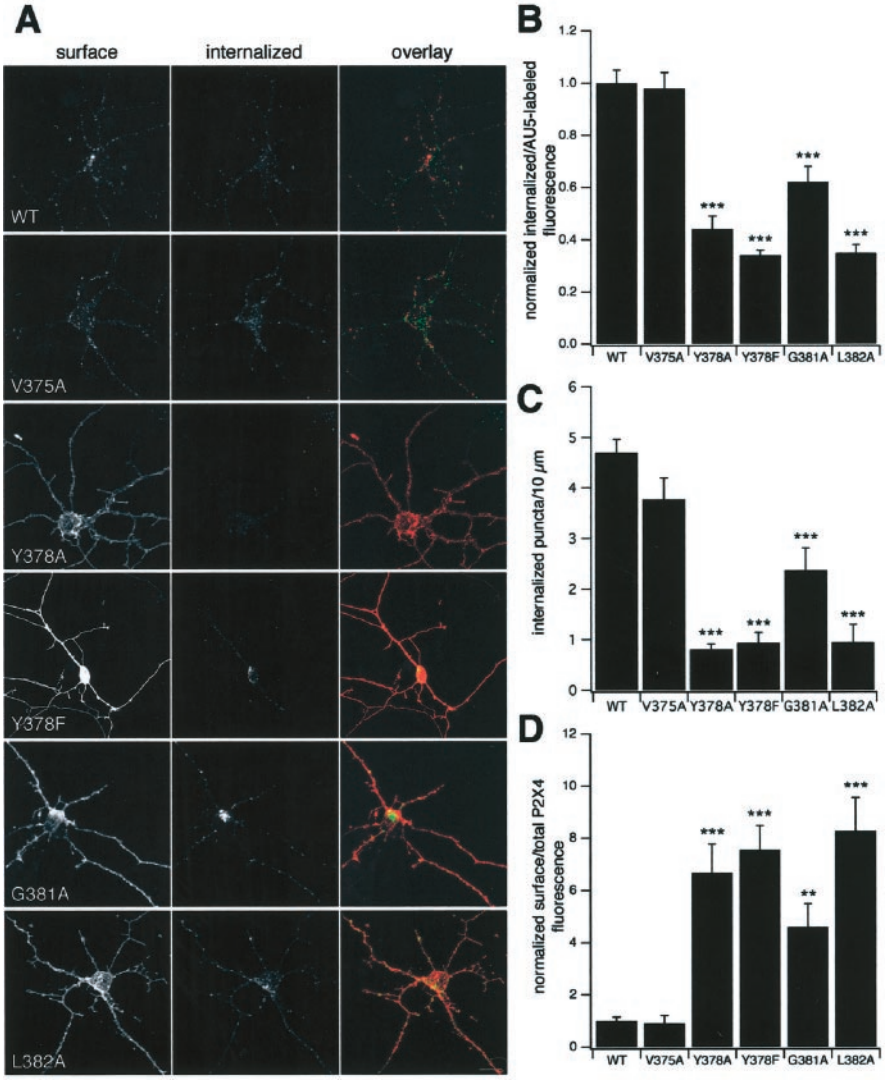

FIG. 3. **Mutation of the Y*XXG*L motif decreases P2X$_4$ receptor internalization and increases surface expression.** *A*, live labeling of P2X$_4$(AU5) and related mutant receptors with anti-AU5 antibody for 30 min at 37 °C. Cell-surface (*left panels*) and internalized (*middle panels*) receptors were visualized using Cy3- and FITC-conjugated secondary antibodies, before and after permeabilization, respectively. For each receptor, a vertical stack of confocal images is shown as a three-dimensional reconstruction. *Scale bar* = 10 μm. *B* and *C*, quantification of P2X$_4$(AU5) and related mutant receptor internalization. The histogram in *B* shows the internalized fluorescence as a fraction of AU5-labeled (surface plus internalized) fluorescence, normalized to control cells (n = 31–63). The histogram in *C* shows the frequency of receptor-positive endosomes internalized from the plasma membrane during a 30-min incubation at 37 °C. Data are shown normalized to 10 μm of neurite length (n = 4–14). *D*, quantification of P2X$_4$(AU5) and related mutant receptor surface expression. The histogram shows the proportion of the total P2X$_4$ receptor population at the cell surface (n = 16–58). *WT*, wild-type. **, $p < 0.01$; ***, $p < 0.001$.

(0.34 ± 0.19 and 0.77 ± 0.37 puncta/10 μm, respectively; $p < 0.001$).

We examined which region of the P2X$_4$ C terminus is important for trafficking by deleting 28, 14, and 7 amino acids from the end (CΔ28, CΔ14, and CΔ7, respectively). When GFP-tagged deletion mutants were expressed in neurons, the CΔ28 and CΔ14 mutants had a more uniform distribution than the full-length receptor, and the frequency of puncta was reduced. In contrast, the CΔ7 mutant exhibited a small decrease in puncta frequency that was not statistically significant (3.95 ± 1.26 puncta/10 μm; $p > 0.05$). Deletions at the N terminus (NΔ5 and NΔ14) had no effect on puncta frequency. Thus, the middle C-terminal region appears to possess determinants for P2X$_4$ receptor trafficking.

Identification of Residues Important in P2X$_4$ Receptor Trafficking—To identify the amino acids in this middle C-terminal region that are involved in trafficking, we individually substituted either alanine or phenylalanine for the four tyrosine residues at positions 367, 372, 374, and 378 and for the lysine residues at positions 370 and 371. Only at position 378 did the mutations substantially alter the distribution of the receptor (Fig. 2). Y378A and Y378F reduced the frequency of puncta by between 3- and 4-fold. Similarly, the Y378A mutation in the P2X$_2$(4C) chimeric receptor ablated the internalization conferred by the P2X$_4$ C-terminal region.

Alanine substitutions were made upstream and downstream of Tyr^{378} to identify other residues that might form part of a motif. Substituting alanine for Gly^{381} (Y+3) and Leu^{382} (Y+4) significantly reduced puncta frequency (2.54 ± 0.51 and 2.17 ± 0.31 puncta/10 μm, respectively; $p < 0.001$). In contrast, substituting alanine for Glu^{379} and Gln^{380} at Y+1 and Y+2 had no significant effect on receptor distribution, and neither did alanine substitutions at Val^{375} (Y−3) or at Glu^{376} and Asp^{377} (Y−2 and Y−1). Thus, the motif is of the form Y*XXG*L.

Mutation of the Endocytic Motif of the P2X$_4$ Receptor Decreases Internalization—To directly measure the effects of the mutations on receptor internalization, GFP was removed from the C terminus, and an AU5 epitope was introduced into the extracellular loop to enable surface receptors in live neurons to be labeled. We previously showed that the introduction of this epitope produces a small shift in the concentration-effect curve for ATP, but does not otherwise alter the function or subcellular distribution of the receptor (7). Receptors at the surface and those that had subsequently been internalized were detected with Cy3- and FITC-conjugated secondary antibodies, respectively (Fig. 3*A*). Cells were analyzed by determining the fraction of labeled receptors that were internalized at the soma (7, 14) and by counting the number of receptor puncta that were internalized during the labeling period in neurites (24).

Mutation of Tyr^{378}, Gly^{381}, or Leu^{382} significantly reduced the proportion of surface receptors that were internalized. In contrast, the V375A mutation had no effect (Fig. 3*B*). To ensure that any decrease in internalization was not simply caused by an increase in surface expression and saturation of the endo-

cytic machinery, internalized receptor fluorescence was measured in neurons with a range of surface expression levels. For cells with similar surface staining, there was considerably less internalized receptor fluorescence in those cells expressing the Tyr^{378}, Gly^{381}, and Leu^{382} mutant receptors compared with the wild-type receptor (see Supplemental Fig. 1). The frequency of internalized puncta for the Tyr^{378} and Leu^{382} mutants was reduced by ~5-fold compared with the wild-type receptor (Fig. 3*C*). The more conservative Y378F mutation was as disruptive as the Y378A mutation, whereas the G381A mutation caused only a 2-fold decrease in internalized puncta frequency. Together, these results suggest that Tyr^{378}, Gly^{381}, and Leu^{382} form a non-canonical tyrosine-based endocytic motif.

Mutation of the Endocytic Motif of the P2X$_4$ Receptor Increases Surface Expression—One of the clearest effects of the Tyr^{378}, Gly^{381}, and Leu^{382} mutations was to increase surface immunolabeling (Fig. 3*A*). To test whether this was caused either by an increase in the overall expression of the receptor in the cell or by an increase in the proportion of receptors at the surface, we compared surface (anti-AU5 antibody) with total (anti-P2X$_4$ antibody) receptor immunofluorescence. Mutation of Tyr^{378}, Gly^{381}, or Leu^{382} caused between a 5- and 8-fold increase in the proportion of the total receptors that were at the surface (Fig. 3*D*). In fact, when we compared the mean total receptor fluorescence for the mutant and wild-type receptors, we found no significant difference in the amount of total receptor ($p = 0.097$, analysis of variance). Thus, mutation of the Y*XX*GL motif increases the surface expression of P2X$_4$ receptors; this is similar to the effect of coexpressing a dominant-negative mutant of dynamin-1 (7).

Increase in the Functional Pool of P2X$_4$ Receptors by Mutation of the Endocytic Motif—Whole-cell patch-clamp recordings were made from HEK293 cells expressing wild-type and mutant P2X$_4$ receptors to determine, first, whether or not the mutants were functional and, second, whether the increase in surface expression was matched by an increase in functional expression (Fig. 4). For these experiments, the receptors were not tagged with either GFP or an AU5 epitope. All of the mutants that we tested were functional, and the time courses of the inward currents in response to 100 μM ATP were similar to those of wild-type P2X$_4$. In each case, there was a biphasic decay in the continued presence of agonist, and the time constants of the fast and slow components were not significantly altered (Fig. 4*A*). There was, however, a significant increase in the peak current density for the Y378A, Y378F, G381A, and L382A mutants compared with either the wild-type or V375A mutant receptor (Fig. 4*B*). Thus, a consequence of inhibiting receptor internalization is the increase in the functional response to application of ATP. This increase was not as great as the increase in surface expression of receptors (2.5-fold *versus* 5–8-fold), suggesting that the proportion of surface receptors that were functional was reduced.

Mutation of the Endocytic Motif Blocks Agonist-regulated Internalization of P2X$_4$ Receptors—To test whether or not agonist-regulated internalization and constitutive internalization occur via a similar mechanism, we compared the effects of ATP on the wild-type and mutant AU5-tagged receptors. After labeling surface receptors with anti-AU5 antibody, neurons were incubated for 15 min at 37 °C with or without 100 μM ATP. ATP caused a 1.5-fold increase in the number of P2X$_4$ receptors that were internalized, whereas it had no effect on the distribution of the Y378A or L382A mutant (Fig. 5). This suggests either that agonist binding promotes the interaction between the Y*XX*GL motif and components of the endocytic machinery or that it slows the subsequent recycling of internalized receptors.

Interaction between the C Terminus of P2X$_4$ and AP-2—

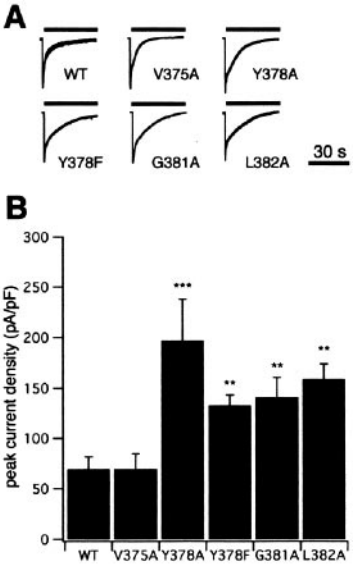

FIG. 4. **Internalization-deficient P2X$_4$ receptors have greater functional expression.** *A*, representative traces showing the response of each receptor to 100 μM ATP (*black bars*). ATP-induced currents were normalized to compare the time course of desensitization. The decay was biphasic (τ_{fast} = 1.15 ± 0.15, 1.17 ± 0.21, 1.57 ± 0.33, 0.86 ± 0.07, 1.34 ± 0.36, and 1.17 ± 0.19 s and τ_{slow} = 8.44 ± 2.64, 7.62 ± 0.70, 13.32 ± 2.87, 11.06 ± 2.14, 11.50 ± 2.02, and 10.23 ± 2.77 s for the wild-type receptor (*WT*) (n = 7), V375A (n = 4), Y378A (n = 4), Y378F (n = 5), G381A (n = 9), and L382A (n = 9), respectively). *B*, summary of electrophysiological data comparing the peak current densities for untagged P2X$_4$ and related mutant receptors. Whole-cell currents were recorded from HEK293 cells expressing untagged P2X receptors in response to application of 100 μM ATP (n = 7–15). *pF*, picofarads. **, $p < 0.01$; ***, $p < 0.001$.

Internalization of P2X$_4$ receptors from the plasma membrane is by a dynamin-dependent mechanism (7). We next investigated whether or not P2X$_4$ receptor internalization occurs via a clathrin- and AP-2-dependent pathway. CCVs were isolated from rat brain using an established protocol (22). We probed the CCV and smooth vesicle fractions as well as the P3 fraction, which contained membranes and cytoskeletal components, with antibodies to P2X$_4$, P2X$_2$, P2X$_7$, GluR1, and α-adaptin (Fig. 6*A*). Immunoblotting with anti-α-adaptin antibody confirmed that the CCV fraction was enriched with AP-2. P2X$_4$ was predominantly in the CCV fraction, as was GluR1. In contrast, we found only a weak signal for P2X$_2$ in both the smooth vesicle and CCV fractions, and there was no detectable band with anti-P2X$_7$ antibody. All receptors were detected in the P3 fraction, suggesting that a lack of detection was not a problem with the antibodies.

To investigate the interaction of the C terminus of P2X$_4$ with AP-2, we expressed the P2X$_4$ C terminus as a soluble GST fusion protein (GST-4C). Purified GST or GST-4C protein was immobilized on glutathione-Sepharose beads and incubated with detergent-solubilized neonatal rat brain extracts. Associated proteins were separated by SDS-PAGE and probed using an antibody to α-adaptin (Fig. 6*B*). GST-4C (but not GST alone) was found to interact with α-adaptin. Together, these observations strongly suggest that P2X$_4$ receptors are endocytosed via a clathrin-dependent pathway *in situ* and that AP-2 recruits P2X$_4$ prior to internalization.

Expression of a Dominant-negative μ2 Subunit Inhibits P2X$_4$ Receptor Internalization—Tyrosine-based sorting motifs have been shown to bind to the μ2 subunit of AP-2 (11). To test whether or not μ2 is involved in P2X$_4$ receptor internalization, we used a dominant-negative μ2 subunit that has two mutations involving key residues necessary for binding canonical

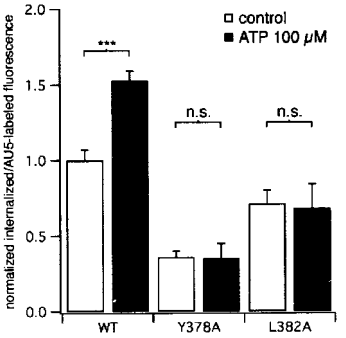

FIG. 5. **Mutation of the endocytic motif ablates agonist-regulated internalization of $P2X_4$ receptors.** The histogram shows the internalized fluorescence as a fraction of total labeled (surface plus internalized) fluorescence, normalized to control cells. ATP-dependent P2X receptor internalization was measured by live labeling transfected neurons for 30 min at 37 °C with anti-AU5 antibody. Cell-surface and internalized receptors were stained following a 15-min application of 100 μM ATP (n = 6–20). *n.s.*, not significant. ***, $p < 0.001$.

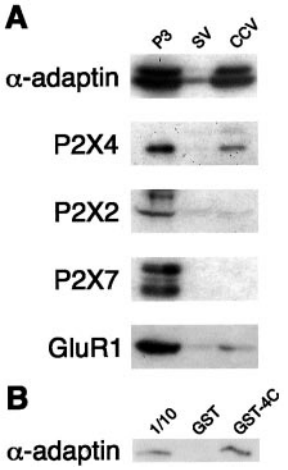

FIG. 6. **$P2X_4$ is present in clathrin-coated vesicles from rat brain, and its C terminus interacts with the AP-2 complex *in vitro*.** *A*, Western blots showing the presence or absence of α-adaptin, $P2X_4$, $P2X_2$, $P2X_7$, and GluR1 in the CCV fraction from rat brain. *B*, the C terminus of $P2X_4$ binds to AP-2. Binding of AP-2 to GST or GST-4C was detected by ECL immunoblotting for α-adaptin. 10% of the amount of extract used for binding was also loaded as a positive control (labeled *1/10*). For *A* and *B*, a representative result from a single experiment is shown. *SV*, smooth vesicle.

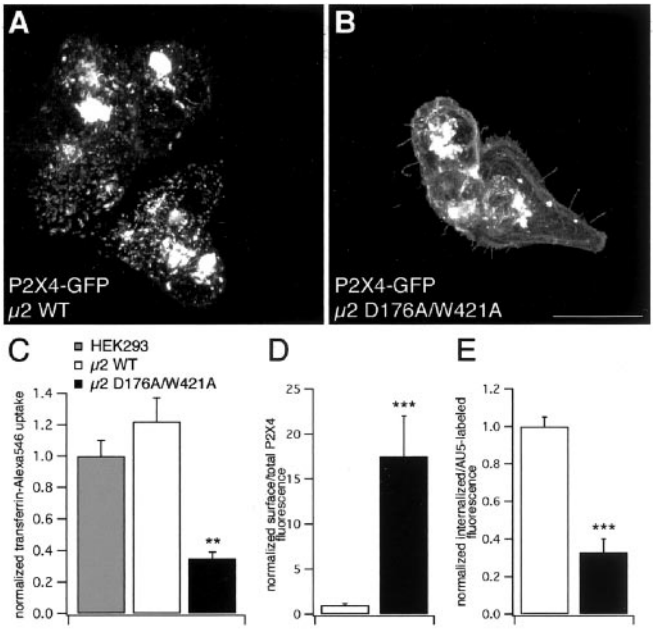

FIG. 7. **Decrease in $P2X_4$ receptor endocytosis in cells expressing the dominant-negative μ2 subunit.** HEK293 cells stably expressing either wild-type (*WT*) (*A*) or D176A/W421A mutant (*B*) μ2 were transiently transfected with $P2X_4$-GFP. Note the redistribution of $P2X_4$-GFP receptors to the plasma membrane in cells expressing D176A/W421A mutant μ2. *Scale bar* = 10 μm. The histogram in *C* shows transferrin uptake in untransfected HEK293 cells or in HEK293 cells stably expressing either wild-type or D176A/W421A mutant μ2. Grayscale values were normalized to the mean value for untransfected HEK293 cells (n = 12–13). The histogram in *D* shows the proportion of the total $P2X_4$(AU5) receptor population that was at the cell surface in cells expressing wild-type or D176A/W421A mutant μ2 (n = 13 or 17, respectively). The histogram in *E* shows internalization of $P2X_4$(AU5) receptors in cells expressing wild-type or D176A/W421A mutant μ2 (n = 11 or 18, respectively). **, $p < 0.01$; ***, $p < 0.001$.

tyrosine-based sorting motifs (D176A/W421A) (12, 19). We generated stable HEK293 cell lines expressing either wild-type or dominant-negative μ2 and showed that the uptake of transferrin/Alexa 568 was significantly reduced in the dominant-negative μ2-expressing cells (Fig. 7*C*). We then compared the subcellular distribution of $P2X_4$-GFP transiently transfected into the two stable cell lines. In cells expressing the dominant-negative μ2 subunit, there was considerably more $P2X_4$-GFP fluorescence associated with the plasma membrane (Fig. 7*B*). In cells expressing the wild-type μ2 subunit, the $P2X_4$ receptor was predominantly in intracellular compartments (Fig. 7*A*); this is consistent with our previous results using wild-type HEK293 cells (7). We next carried out live labeling of $P2X_4$(AU5) receptors expressed in the two stably transfected cell lines and found that, in the presence of dominant-negative μ2, there was a 16-fold increase in the fraction of the total receptor population that was at the surface (Fig. 7*D*). There was also a 3-fold decrease in the internalization of anti-AU5 antibody-labeled surface receptors (Fig. 7*E*). Thus, the internalization of $P2X_4$ receptors appears to involve an interaction between the Y*XX*GL motif and the tyrosine-binding pocket of μ2.

DISCUSSION

The results presented here demonstrate that the ionotropic $P2X_4$ receptor contains a non-canonical tyrosine-based sorting motif in its C terminus, Y*XX*GL. This sorting signal is important for constitutive internalization and agonist-regulated internalization, indicating that they involve a common mechanism. Targeted mutation of the motif or of the tyrosine-binding pocket of the μ2 subunit of AP-2 caused an increase in surface receptor number. The increase in surface receptor number with mutant $P2X_4$ receptors was associated with an increase in the functional pool of receptors. Thus, constitutive internalization is important for determining receptor density.

Interaction between YXXGL and the μ2 Subunit—Together, our data suggest that the C terminus of $P2X_4$ interacts with AP-2 via a non-canonical tyrosine-based motif of the form Y*X*-*X*GL by binding to the μ2 subunit. We propose that, like Y*XX*Ø motifs, Tyr^{378} and Leu^{382} of $P2X_4$ fit into the two hydrophobic binding pockets on either side of strand β16 (12, 25, 26). If the C terminus of $P2X_4$ were in an extended conformation, this fit would not be favorable. However, we found that Gly^{381} could not be substituted with an alanine residue without an impairment of internalization. This subtle change in side chain is predicted to greatly affect the flexibility of the peptide (27). Thus, a glycine (but not an alanine) residue at Y+3 may allow Leu^{382} to fit into the second hydrophobic pocket.

Non-canonical Tyrosine-based Sorting Motifs—Tyrosine-based sorting motifs are a family of degenerate signals that can often be minimally described by a critical tyrosine residue that cannot be substituted by alanine or phenylalanine (11). Amino acids with bulky hydrophobic side chains are also often re-

TABLE I
Identification of similar motifs in the C terminal of other polytopic membrane proteins

Name	Swiss-Prot accession no.	Sequence	Positions
P2X purinoceptor 4 (P2X$_4$)	P51577	**YEQGL**	378–382
GluR2	P19491	**YKEGY**	869–873
GluR3	P19492	**YREGY**	874–878
Inward rectifier K^+ channel Kir2.3 (BIR11)	P52190	**YDIGL**	246–250
Adenosine A2a receptor	P30543	**YTLGL**	356–360
β_2-Adrenergic receptor	P10608	**YGNGY**	350–354
Cannabinoid receptor-2 (CB-2)	Q9QZN9	**YLQGL**	320–324

quired for the interaction with μ2, usually at Y+3. Indeed, μ2 was identified as an interacting protein using a Y*XX*Ø signal (28). Using a combinatorial approach, Boll *et al.* (29) documented the preference of GST-μ2 for peptides of the form *XXXX*Y*XXXX*. The optimal sequence for μ2 binding was found to be Y*X*RL. However, the selection of glycine at Y+3 was similar to that for more bulky hydrophobic residues, whereas the selection of alanine at Y+3 was very low (29). Other studies have also shown that alanine at Y+3 is not compatible with a μ2 interaction (28, 30).

There is a precedent for a tyrosine-based sorting motif with a bulky hydrophobic residue at Y+4. The thromboxane A$_2$ receptor is a G-protein-coupled receptor that requires a Y*XXX*I signal for tonic (but not agonist- induced) internalization (31). This signal differs from Y*XX*GL in that it has Thr at Y+3, not Gly. It is also not established whether or not this receptor is endocytosed following an interaction with μ2.

In the absence of a bulky hydrophobic residue at Y+3, amino acids with bulky hydrophobic side chains at Y−3 have also been reported to be important for μ2 binding (26). However, we found that a valine residue at Y−3 in P2X$_4$ was not required for endocytosis.

It is not known exactly how selectivity for different Y*XX*Ø signals is achieved by AP-2. One hypothesis is that subtle differences in the residues at each Y+1 and Y+2 could confer selectivity (10). Indeed, there is structural evidence to indicate that Arg at Y+2 in TGN-38 makes multiple contacts with μ2 and strengthens the interaction (12). However, the Y*XX*GL signal is not predicted to make such contacts with μ2. Because of potential differences in binding, this new type of motif could provide a basis for differential selection of receptor molecules by AP-2. This raises several key questions, *i.e.* are Y*XX*Ø motif- and Y*XX*GL motif-containing receptors trafficked in distinct endosomal compartments, or can they share the same clathrin-coated vesicle?

Trafficking of P2X Receptors—The Y*XX*GL motif is totally conserved among mammalian P2X$_4$ sequences (YEQGL), but is absent from other P2X receptor subtypes. Of the subtypes tested so far, P2X$_4$ (but not P2X$_2$ or P2X$_6$) receptors constitutively cycle between the plasma membrane and intracellular compartments (7). P2X$_1$ receptors have been reported to undergo agonist-mediated internalization (32, 33), but it is not clear if any basal P2X$_1$ internalization occurs. In addition, the molecular requirements for P2X$_1$ endocytosis are currently unknown. For P2X$_7$ receptors, some intracellular staining for P2X$_7$ protein in neurons has been observed (34), suggesting endocytic uptake of native receptors; yet we failed to detect any P2X$_7$ immunoreactivity in the CCV fraction isolated from rat brain.

Identification of Similar Motifs in Other Receptors and Ion Channels—The new type of tyrosine-based endocytic motif identified here may be present in other transmembrane proteins and be important in regulating their surface number. Table I shows selected results from a search for motifs similar to Y*XX*GL in other membrane proteins cloned from *Rattus norvegicus* in the Swiss Protein Database. The search was performed with ScanProsite[3] and used Y*XX*GØ (in Prosite format Y-x(2)-G-[LIVMFY]). A Y*XX*GØ sequence was found in 634 entries. Of these, 105 were transmembrane proteins, and 19 had the motif present in an intracellular domain. Of particular note are the entries for the AMPA receptor subunits GluR2 and GluR3. AMPA receptors have previously been shown to use the internalization machinery to modify surface receptor number (6, 14, 15, 35). The precise sequence requirements for AMPA receptor endocytosis are presently unknown, however (2, 14). We propose therefore that non-canonical tyrosine-based endocytic motifs may be involved in the control of the surface number of other receptors and ion channels.

Acknowledgments—We thank Dr. D. J. Owen for discussions regarding the P2X$_4$-μ2 interaction, Dr. M. S. Robinson for the μ2 cDNA, and Dr. F. Araujo and J. G. Carlton for help in generating the μ2 and GST constructs.

REFERENCES

1. Carroll, R. C., Beattie, E. C., von Zastrow, M., and Malenka, R. C. (2001) *Nat. Rev. Neurosci.* **2,** 315–324
2. Sheng, M., and Lee, S. H. (2001) *Cell* **105,** 825–828
3. Moss, S. J., and Smart, T. G. (2001) *Nat. Rev. Neurosci.* **2,** 240–250
4. Turrigiano, G. G. (2000) *Neuron* **26,** 5–8
5. Burrone, J., and Murthy, V. N. (2001) *Curr. Biol.* **11,** R274–R277
6. Man, H. Y., Lin, J. W., Ju, W. H., Ahmadian, G., Liu, L. D., Becker, L. E., Sheng, M., and Wang, Y. T. (2000) *Neuron* **25,** 649–662
7. Bobanovic, L. K., Royle, S. J., and Murrell-Lagnado, R. D. (2002) *J. Neurosci.* **22,** 4814–4824
8. Kittler, J. T., Delmas, P., Jovanovic, J. N., Brown, D. A., Smart, T. G., and Moss, S. J. (2000) *J. Neurosci.* **20,** 7972–7977
9. Marsh, M., and McMahon, H. T. (1999) *Science* **285,** 215–220
10. Kirchhausen, T. (1999) *Annu. Rev. Cell Dev. Biol.* **15,** 705–732
11. Bonifacino, J. S., and Dell'Angelica, E. C. (1999) *J. Cell Biol.* **145,** 923–926
12. Owen, D. J., and Evans, P. R. (1998) *Science* **282,** 1327–1332
13. Carroll, R. C., Beattie, E. C., Xia, H. H., Luscher, C., Altschuler, Y., Nicoll, R. A., Malenka, R. C., and von Zastrow, M. (1999) *Proc. Natl. Acad. Sci. U. S. A.* **96,** 14112–14117
14. Lin, J. W., Ju, W., Foster, K., Lee, S. H., Ahmadian, G., Wyszynski, M., Wang, Y. T., and Sheng, M. (2000) *Nat. Neurosci.* **3,** 1282–1290
15. Wang, Y. T., and Linden, D. J. (2000) *Neuron* **25,** 635–647
16. Roche, K. W., Standley, S., McCallum, J., Dune Ly, C., Ehlers, M. D., and Wenthold, R. J. (2001) *Nat. Neurosci.* **4,** 794–802
17. Ehlers, M. D. (2000) *Neuron* **28,** 511–525
18. Khakh, B. S., Burnstock, G., Kennedy, C., King, B. F., North, R. A., Seguela, P., Voigt, M., and Humphrey, P. P. (2001) *Pharmacol. Rev.* **53,** 107–118
19. Nesterov, A., Carter, R. E., Sorkina, T., Gill, G. N., and Sorkin, A. (1999) *EMBO J.* **18,** 2489–2499
20. Koizumi, S., Bootman, M. D., Bobanoviæ, L. K., Schell, M. J., Berridge, M. J., and Lipp, P. (1999) *Neuron* **22,** 125–137
21. Hamill, O. P., Marty, A., Neher, E., Sakmann, B., and Sigworth, F. J. (1981) *Pfluegers Arch.* **391,** 85–100
22. Campbell, C., Squicciarini, J., Shia, M., Pilch, P. F., and Fine, R. E. (1984) *Biochemistry* **23,** 4420–4426
23. Laemmli, U. K. (1970) *Nature* **227,** 680–685
24. Snyder, E. M., Philpot, B. D., Huber, K. M., Dong, X., Fallon, J. R., and Bear, M. F. (2001) *Nat. Neurosci.* **4,** 1079–1085
25. Follows, E. R., McPheat, J. C., Minshull, C., Moore, N. C., Pauptit, R. A., Rowsell, S., Stacey, C. L., Stanway, J. J., Taylor, I. W., and Abbott, W. M. (2001) *Biochem. J.* **359,** 427–434
26. Owen, D. J., Setiadi, H., Evans, P. R., McEver, R. P., and Green, S. A. (2001) *Traffic* **2,** 105–110
27. Ramachandran, G. N., and Sasisekharan, V. (1968) *Adv. Protein Chem.* **23,** 283–438
28. Ohno, H., Stewart, J., Fournier, M. C., Bosshart, H., Rhee, I., Miyatake, S., Saito, T., Gallusser, A., Kirchhausen, T., and Bonifacino, J. S. (1995) *Science* **269,** 1872–1875
29. Boll, W., Ohno, H., Songyang, Z., Rapoport, I., Cantley, L. C., Bonifacino, J. S., and Kirchhausen, T. (1996) *EMBO J.* **15,** 5789–5795

[3] Available at ca.expasy.org/tools/scnpsite.html.

30. Ohno, H., Fournier, M. C., Poy, G., and Bonifacino, J. S. (1996) *J. Biol. Chem.* **271,** 29009–29015
31. Parent, J. L., Labrecque, P., Driss Rochdi, M., and Benovic, J. L. (2001) *J. Biol. Chem.* **276,** 7079–7085
32. Li, G. H., Lee, E. M., Blair, D., Holding, C., Poronnik, P., Cook, D. I., Barden, J. A., and Bennett, M. R. (2000) *J. Biol. Chem.* **275,** 29107–29112
33. Ennion, S. J., and Evans, R. J. (2001) *FEBS Lett.* **489,** 154–158
34. Deuchars, S. A., Atkinson, L., Brooke, R. E., Musa, H., Milligan, C. J., Batten, T. F., Buckley, N. J., Parson, S. H., and Deuchars, J. (2001) *J. Neurosci.* **21,** 7143–7152
35. Luscher, C., Xia, H. H., Beattie, E. C., Carroll, R. C., von Zastrow, M., Malenka, R. C., and Nicoll, R. A. (1999) *Neuron* **24,** 649–658